Cell Reports

Article

Cytoplasmic DIS3 is an exosome-independent endoribonuclease with catalytic activity toward circular RNAs

Graphical abstract

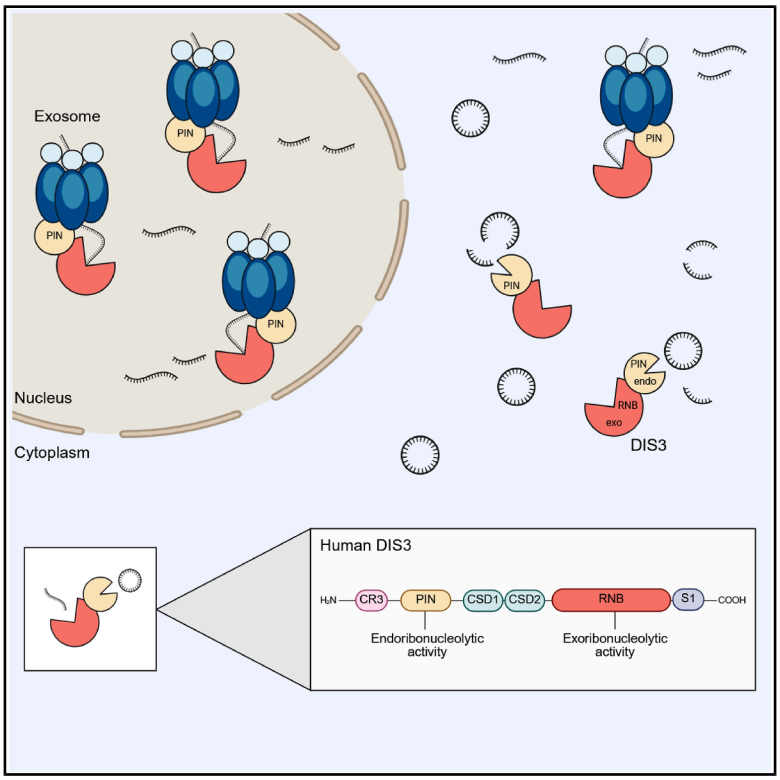

Highlights

- Biochemical fractionations identify human DIS3 as circRNA endonucleases
- The PIN domain of DIS3 cleaves naturally occurring circRNAs *in vitro*
- DIS3 partially resides in the cytoplasm of human cells
- Cytoplasmic DIS3 functions as a stand-alone endoribonuclease independently of the exosome

Authors

Claudia Latini, Julian Eichlinger, Anna-Lisa Fuchs, ..., Li Yang, Remco Sprangers, Gunter Meister

Correspondence

gunter.meister@ur.de

In brief

CircRNAs are generated during splicing, but their specific degradation pathways are poorly understood. Latini et al. identify and biochemically characterize the exo- and endoribonuclease DIS3 as a candidate for cytoplasmic circRNA degradation. DIS3 uses its catalytic PIN domain to cleave circRNAs and functions in the cytoplasm independently of the exosome.

Latini et al., 2025, Cell Reports *44*, 115769
June 24, 2025
https://doi.org/10.1016/j.celrep.2025.115769

CellPress

Cell Reports

CellPress
OPEN ACCESS

Article

Cytoplasmic DIS3 is an exosome-independent endoribonuclease with catalytic activity toward circular RNAs

Claudia Latini,[1] Julian Eichlinger,[1] Anna-Lisa Fuchs,[2] Si-Nan Zhai,[3,4] Hung Ho-Xuan,[1] Gerhard Lehmann,[1] Petar Glažar,[5] Nikolaus Rajewsky,[5] Astrid Bruckmann,[1] Li Yang,[3] Remco Sprangers,[2] and Gunter Meister[1,6,*]

[1]Regensburg Center for Biochemistry (RCB), Laboratory for RNA Biology, University of Regensburg, 94053 Regensburg, Germany
[2]Regensburg Center for Biochemistry (RCB), Institute of Biophysics and Physical Biochemistry, University of Regensburg, 93053 Regensburg, Germany
[3]Center for Molecular Medicine, Children's Hospital of Fudan University and Shanghai Key Laboratory of Medical Epigenetics, International Laboratory of Medical Epigenetics and Metabolism, Ministry of Science and Technology, Institutes of Biomedical Sciences, Fudan University, Shanghai 200032, China
[4]Shanghai Institute of Nutrition and Health, University of Chinese Academy of Sciences, Chinese Academy of Sciences, Shanghai 200031, China
[5]Laboratory for Systems Biology of Gene Regulatory Elements, Berlin Institute for Medical Systems Biology, Berlin, Germany
[6]Lead contact
*Correspondence: gunter.meister@ur.de
https://doi.org/10.1016/j.celrep.2025.115769

SUMMARY

The ribonuclease DIS3 interacts through its PIN domain with the nuclear exosome and degrades linear RNA substrates using its exoribonuclease domain. However, the PIN domain is also an active endoribonuclease, but cellular substrates are largely unknown. Here, we use a biochemical strategy to find ribonucleases that could degrade circular RNAs (circRNAs). Due to the lack of accessible ends, circRNAs are resistant to exonucleolytic cleavage and are thus more stable than linear RNAs. Using biochemical assays, we identify DIS3 as a candidate for circRNA degradation and demonstrate that it partially resides in the cytoplasm, where circRNAs are degraded. DIS3 shows cleavage activity toward a number of circRNAs and functions independently of the exosome core *in vitro*. Upon knockdown of DIS3 in cell lines, selected circRNAs are moderately stabilized. We thus propose that cytoplasmic DIS3 functions as a stand-alone enzyme independently of the exosome core and may contribute to circRNA turnover.

INTRODUCTION

Circular RNAs (circRNAs) are generated during splicing of pre-mRNA molecules and have been found in a large variety of species including humans.[1] In canonical splicing processes, a 5′ splice site finds a downstream 3′ splice site leading to the removal of the intron.[2] CircRNAs result from back-splicing when a 5′ splice site splices "back" on an upstream 3′ splice site resulting in a circular transcript containing the sequences located between these two splice sites. The identification of numerous different and low-abundant circRNAs suggests pervasive back-splicing. However, some circRNAs also accumulate to higher cellular concentrations, and factors such as complementarity between the two flanking introns or RNA-binding proteins (RBPs) that bring two introns in close proximity through dimerization, for example, may contribute to promoting back-splicing and circRNA generation.[1] Alterations of splicing and transcription dynamics directly affect circRNA output, suggesting that the timing and the availability of splice sites is an important feature of back-splicing, which may lead to a widespread, low-abundant circRNA production.[3,4]

Many circRNAs have acquired cellular functions. The circRNA Cdr1as contains multiple binding sites for miR-7 and functions as a sponge for this microRNA.[5,6] Sponging functions for RBPs and direct interactions with other RNAs have been reported.[7] Furthermore, circRNA may also contain open reading frames, and indeed, some circRNAs generate protein products.[8,9] Given the broader generation of circRNAs from the cellular transcriptome, circRNAs are also specific to diseases including cancer.[10] In most cases, however, it remains elusive whether these circRNAs are causally expressed or a consequence of the respective gene expression programs.

While many functions of circRNAs are still a matter of debate, it is rather clear that they need to be turned over by cellular pathways as any other RNA class. Several endoribonucleases have been found to degrade circRNAs. Upon viral infection, RNase L is activated to degrade cellular and viral RNAs. This 2′-5′ oligoadenylate-synthase (oligoadenylate synthetase [OAS])/RNase L pathway is triggered by viral double-stranded RNA. Interestingly, many circRNAs can also form double-stranded regions and act as inhibitors of the protein kinase R (PKR) pathway. Upon viral infection, RNase L degrades

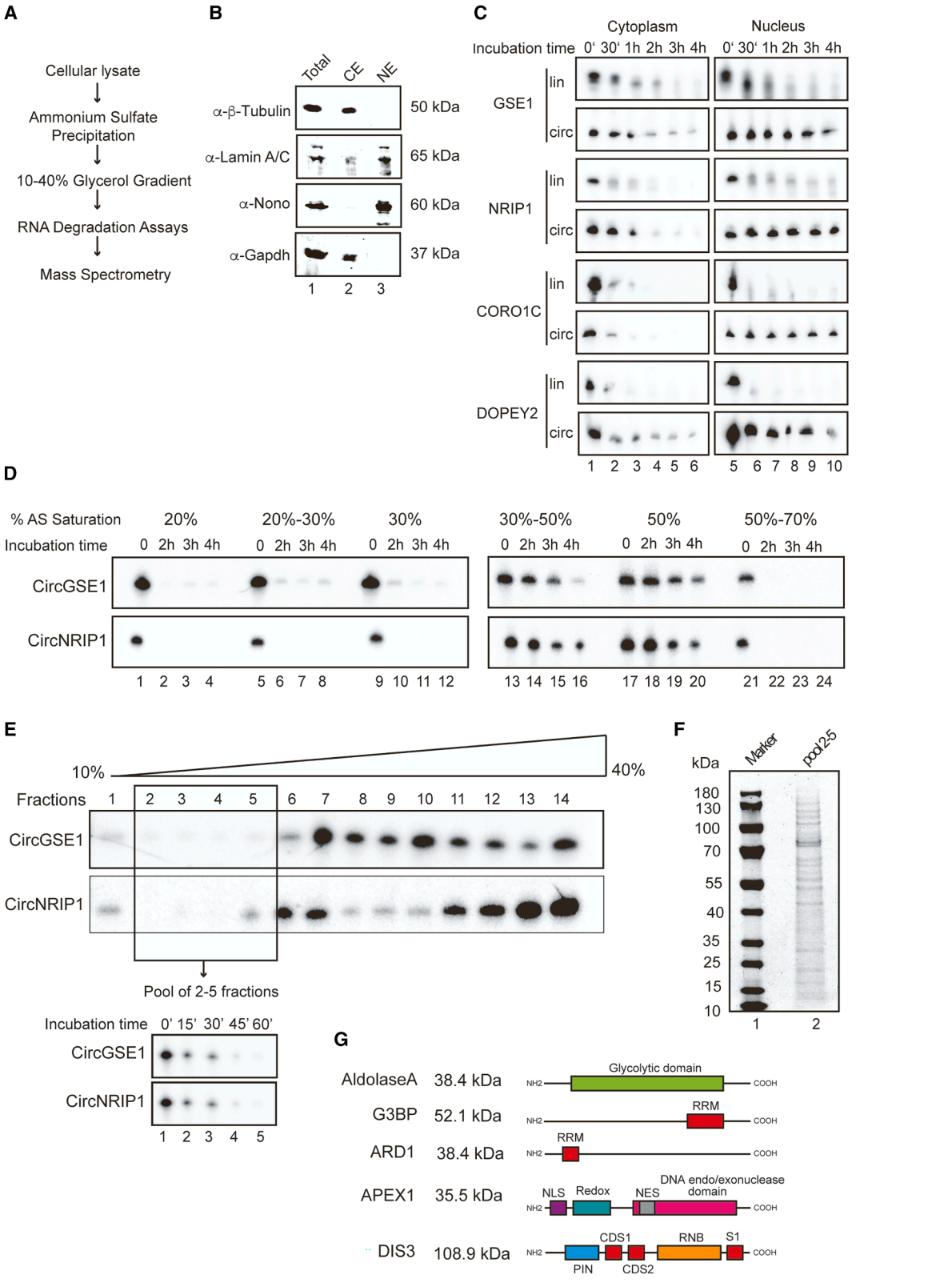

(legend on next page)

circRNAs, and the PKR pathway can be activated.[11] Like many other RNAs, circRNAs can be m^{6}A-modified with consequences for their functions and also stability. The m^{6}A reader protein YTH domain-containing family protein 2 (YTHDF2) can associate with the RNase P/MRP ribonucleoprotein particle (RNP) and cleave such modified circRNAs.[12] Another recent study reported that highly structured RNAs including many 3′ untranslated regions and also circRNAs are degraded by the endoribonuclease Ras GTPase-activating protein-binding protein 1 (G3BP1) in complex with the ATP-dependent RNA helicase upstream frameshift 1 (UPF1).[13] Finally, it is also conceivable that circRNAs are cleared through exocytosis rather than endogenous decay pathways, which would be consistent with the finding of numerous circRNAs in extracellular vesicles circulating in body fluids.[14]

Most of the aforementioned degradation pathways act on circRNAs containing specific features or expression patterns. However, given the widespread expression and broad sequence diversity, we reasoned that housekeeping degradation pathways might be attractive candidates for a broader circRNA reduction. Therefore, we performed a biochemical fractionation approach following cellular degradation activity in lysates. Mass spectrometry of the active fractions identified the endo-/exoribonuclease DIS3, and we demonstrate that this enzyme can degrade endogenous circRNAs *in vitro*. DIS3 knockdown cells show moderate effects on the levels of several circRNAs. Moreover, DIS3 functions independently of the exosome in the cytoplasm, and therefore, we conclude that DIS3 can function as a stand-alone enzyme with catalytic activity toward circRNAs.

RESULTS

DIS3 fractionates with circRNA degradation activity

To find ribonucleases that contribute to circRNA degradation, we followed a biochemical fractionation approach (Figure 1A). We selected circNRIP1, circGSE1, circCORO1C, and circDOPEY2 for our circRNA degradation assays because of their small size, which is suitable for *in vitro* circularization. We confirmed by PCR and RNase R treatment that these RNAs are indeed naturally occurring in HEK293 cells (Figures S1A and S1B; Table S1). For circRNA expression, linear RNAs were *in vitro* transcribed, radiolabeled, and circularized using T4 RNA ligase 1 (Figure S1C). To validate that the slower migrating bands are the desired circularized RNA products, we performed RNase R treatment (Figure S1D). While the faster migrating linear product was readily degraded, the circRNA products were resistant to RNase R. Furthermore, when we used a complementary DNA oligonucleotide and performed RNase H treatment, the linear band was cleaved into two products while the circular RNA resulted in only one band (Figure S1E). These results demonstrate that the slower migrating band is indeed the radiolabeled circularized variant.

As a first fractionation of circRNA-directed degradation activity, we generated nuclear and cytoplasmic extracts (Figure 1B) and incubated the four circRNAs as well as their linear versions with these extracts (Figure 1C). While the linear RNAs were rapidly degraded in both nuclear and cytoplasmic lysates, the circular RNAs were specifically degraded in the cytoplasmic fractions. Cytoplasmic fractions were further separated by ammonium sulfate (AS) precipitation (Figure 1D). Cytoplasmic lysates were incubated with increasing AS concentrations; the precipitates were resolved and incubated with circGSE1 and circNRIP1. Since the nucleolytic activity was readily detectable in the 30% AS precipitate, this fraction was further separated by glycerol density centrifugation ranging from 10% to 40% (Figure 1E). For both circRNAs, the major activity was detected in rather low-molecular-weight fractions, which was confirmed by independent experiments (lower panel). The pooled fractions 2 to 5 were subjected to mass spectrometry and analyzed for proteins containing endonuclease domains (Figures 1F and 1G). Among them, we found aldolase A,[15] a glycolytic protein that has been associated with endoribonuclease activity; G3BP1, a multi-function protein with endoribonucleolytic degradation activity[13]; ARD1, a mammalian analog of *E.coli* RNaseE[15] also known as protein phosphatase 1, regolatory (inhibitor) 8 (PPP1R8); the apurinic/apyridiminic endodeoxyribonuclease 1 APEX1, a protein that functions as DNA endonuclease[15]; and DIS3, a well-characterized exo- and endoribonuclease associated with the exosome.[16]

The PIN domain of DIS3 cleaves circRNAs *in vitro*

We reasoned that a housekeeping endoribonuclease would be an attractive candidate for the various circularized RNAs produced during splicing. Therefore, we focused on DIS3 for further functional studies. DIS3 is highly conserved and possesses an exoribonuclease domain (RNB) as well as an endoribonuclease domain (PIN, Figure 2A). DIS3 associates with the nuclear exosome to provide exoribonuclease activity.[16] However, the activity found in our fractionations is associated with rather low-molecular-weight complexes (Figure 1E). To study the relevance of the core exosome for circRNA degradation, we switched to recombinant yeast proteins. We generated yeast exosome core complexes (Rrp4, 40–43, 45–46, Csl4, and Mtr3) either without

Figure 1. DIS3 is associated with circRNA degradation activity

(A) Schematic representation of the biochemical strategy used to identify circRNA-specific ribonucleases.

(B) Cytoplasmic (CE) and nuclear (NE) extracts from HEK293T cells were analyzed by western blot. β-Tubulin and GAPDH were used as cytoplasmic markers, while Lamin A/C and NONO as nuclear markers.

(C) Circular and linear radiolabeled versions of GSE1, NRIP, CORO1C, and DOPEY2 were incubated with cytoplasmic and nuclear extracts at different time points and analyzed by denaturing RNA polyacrylamide gel electrophoresis (PAGE).

(D) Radiolabeled synthetic circGSE1 and circNRIP1 were incubated with increasing amounts of ammonium sulfate (% AS saturation). AS precipitates from cytoplasmic extracts were used for circRNA cleavage and analyzed by RNA-PAGE.

(E) The 30% AS saturated precipitate was fractionated on a 10%–40% glycerol gradient. The resulting fractions were incubated with radiolabeled circNRIP1 and circGSE1 and analyzed as described above. Lower: fractions 2–5 were pooled, and circRNA degradation activity was validated using shorter incubation time.

(F) Coomassie staining of the proteins present in the pooled fractions 2–5 used for mass spectrometry.

(G) Summary table of the five endoribonucleases identified by mass spectrometry. Domain structures and molecular weights are shown.

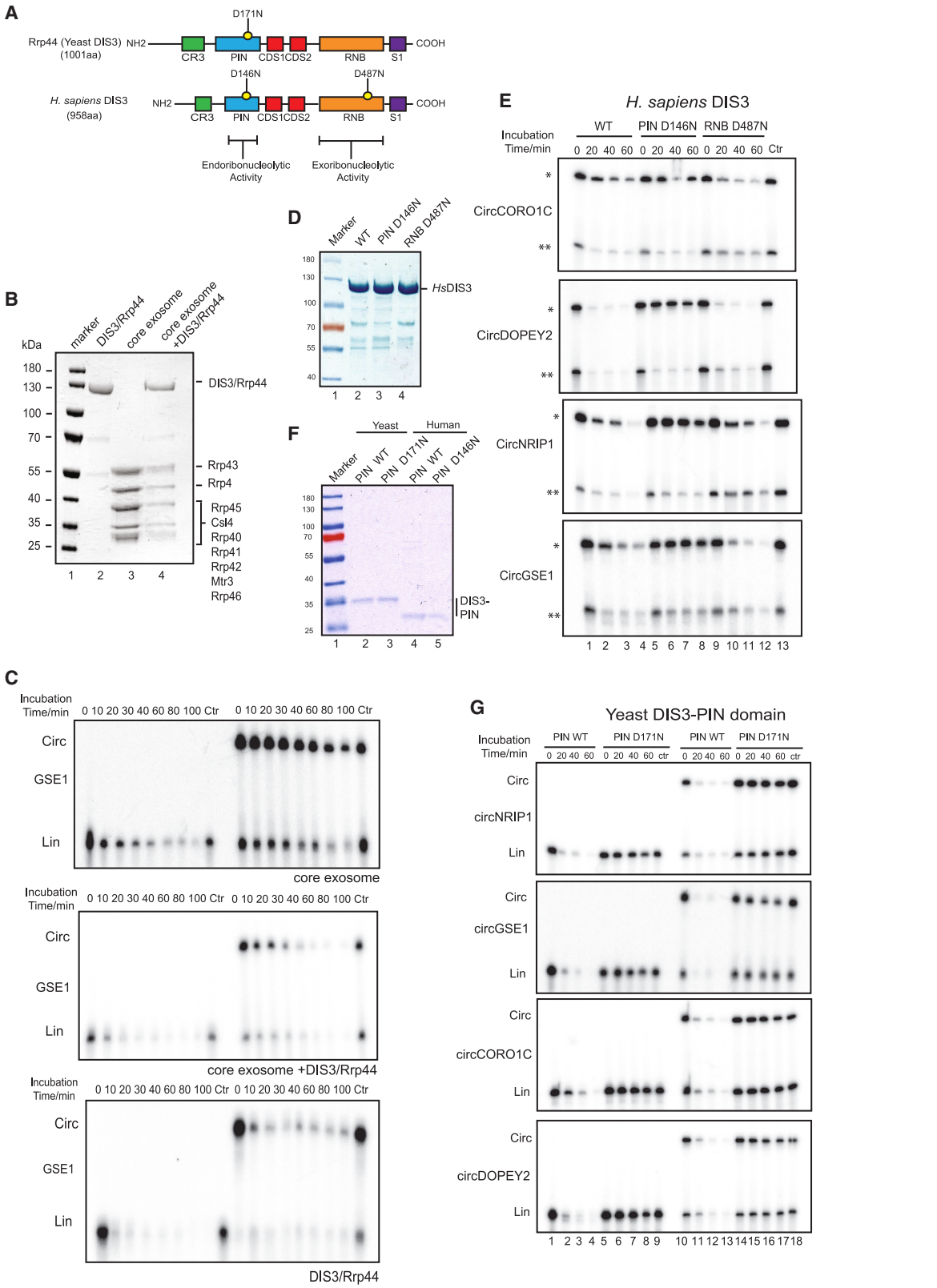

(legend on next page)

(core exosome) or with yeast DIS3 (core exosome + Rrp44) (Figure 2B). The yeast homolog is Rrp44, and, for simplicity, we refer to it as yeast DIS3. Recombinant complexes were incubated with radiolabeled circGSE1, and while the core exosome shows only background cleavage, the addition of yeast DIS3 led to very efficient cleavage of the linear and circular RNA substrates (Figure 2C, upper and middle panels). Interestingly, when we used yeast DIS3 alone (lower panel), similarly efficient cleavage activities were observed suggesting that DIS3 does not require association with the core exosome for endonucleolytic activity and circRNA degradation.

We next tested whether the activity is specific to the PIN domain and whether the isolated PIN domain is sufficient for circRNA cleavage. We mutated the PIN (D146N) and the RNB (D487N) domains individually (Figure 2A), generated recombinant proteins in *E. coli* (Figure 2D), and performed *in vitro* circRNA cleavage assays (Figure 2E). Human wild-type (WT) DIS3, DIS3 D146N (PIN), and DIS3 D487N (RNB) proteins were incubated with circCOROC1C, circDOPEY2, circNRIP1, and circGSE1. Indeed, the PIN domain mutant lost circRNA cleavage activity while both WT and the RNB mutant remained active. Furthermore, the isolated WT yeast DIS3 PIN domain readily cleaved both linear and circular forms of all four tested circRNAs, while the mutant variant neither cleaved linear RNA nor circRNA (Figures 2F and 2G). Similar cleavage activity was obtained for the isolated WT and mutated human DIS3 PIN domains (Figures 2F and S2A). Our results therefore show that DIS3 cleaves natural circRNA substrates *in vitro* and that the PIN domain is responsible for this function.

DIS3 reduction affects expression levels of endogenous circRNAs

To corroborate our findings with yeast and human recombinant proteins (Figure 2) in a more physiological environment, we performed cleavage experiments using immunoprecipitated FLAG/HA (FH)-tagged proteins (Figures 3A and 3B). We isolated several core exosome components as well as DIS3 from HEK293 cell lysates (Figure 3A). Incubation of the immunoprecipitates with circNRIP1 showed clear degradation activity for DIS3 (Figure 3B). All other samples, however, did not show cleavage above background, corroborating our model that DIS3-mediated circRNA cleavage functions independently of the exosome. DIS3L1 served as negative control since it carries a catalytically inactive PIN domain. However, over time, some circNRIP1 decay is reproducibly observed in the DIS3L1 reaction, suggesting that an unknown endonuclease might co-immunoprecipitate. Moreover, another endonuclease candidate, FH-ARD1, showed moderate cleavage activity as well (see discussion), while FH-APEX1 remained inactive (Figure S2B) ruling out general background contaminants in our assays.

DIS3 is an essential gene, and most knockout cells are not viable. To nevertheless inactivate it and test endogenous circRNA levels, we chose a replacement strategy. We stably integrated an inducible tagged DIS3 variant into HEK293 cells using the Flp-In system. We then knocked out the endogenous gene using CRISPR-Cas9. Although low, some leaky expression from the inducible cassette was unavoidable that most likely contributed to cell survival (Figure S3A). Doxycycline induction resulted in strong overexpression of DIS3 (Figure S3B). We refer to these cells as knockdown cells since some DIS3 expression is still present in the uninduced state. In these cells, although the mature 5.8S rRNA is unchanged, pre-5.8S rRNA intermediates partially accumulated, demonstrating delayed 5.8S rRNA maturation, a process that requires nuclear DIS3 activity[17–19] (Figures S3C–S3E). We used these cells to investigate selected circRNA candidates using qPCR in WT, DIS3 knockdown, and DIS3 rescue cells (Figure 3C). Indeed, many circRNAs were moderately upregulated, and rescue through DIS3 induction markedly reduced the levels again (Figure 3C). For a small additional panel of circRNA candidates, we compared these effects to their linear counterparts (Figure 3D). While the four tested circRNAs are upregulated and rescued in the DIS3 knockdown cells, the linear mRNAs are much less affected (Figure 3D). As an additional direct detection approach, we performed northern blotting against one of the endogenous candidates, circular SMO (circSMO) (Figure 3E). Strikingly, circSMO signals appeared much stronger in the knockdown clones, while the linear transcript was rather unchanged. A dox-induced DIS3 rescue experiment showed a similar trend but was probably due to a weaker northern blot sensitivity (data not shown).

Taken together, a number of circRNAs are affected by DIS3 reduction, but our validation experiments do not allow for a deeper analysis of specific features common to these circRNAs and require further structural and functional investigations.

Cytoplasmic human DIS3 functions as a stand-alone enzyme to degrade circRNAs

Human DIS3 localizes mainly to the nucleus and associates with the exosome to process nuclear RNAs.[16] However, we find that activity in cytoplasmic lysates and a minor cytoplasmic DIS3 portion has been observed before.[20] We therefore tested the subcellular localization of DIS3 and the investigated circRNAs in our cellular and biochemical systems. First, we performed

Figure 2. DIS3 uses its PIN domain to degrade circRNAs *in vitro* independently of the exosome

(A) Domain organization of human DIS3 and Rrp44 (yeast DIS3). Mutations of conserved aspartates that abolish DIS3 ribonucleolytic activities are indicated.

(B) Coomassie staining of purified recombinant yeast DIS3/Rrp44, the core exosome complex, and the core exosome complex including yeast DIS3/Rrp44.

(C) Cleavage reactions using radiolabeled linear and circular GSE1 together with the recombinant proteins shown in (B). Of note, spontaneous hydrolyzation of circRNAs frequently generates a linear RNA band in purified circRNA samples.

(D) Coomassie staining showing different versions of recombinant human DIS3 protein: wild-type DIS3 (WT), PIN domain mutant (DIS3D146N), and the exoribonuclease mutant (DIS3D487N).

(E) Cleavage assays using radiolabeled circNRIP1, circGSE1, circCORO1C, and circDOPEY2 RNAs (*) incubated with proteins shown in (D). Linear substrate molecules resulting from spontaneous breakage of circularized RNAs are indicated with **.

(F) Coomassie staining showing the yeast and human recombinant WT PIN domains and their respective mutants.

(G) Cleavage assays using the yeast proteins shown in (F).

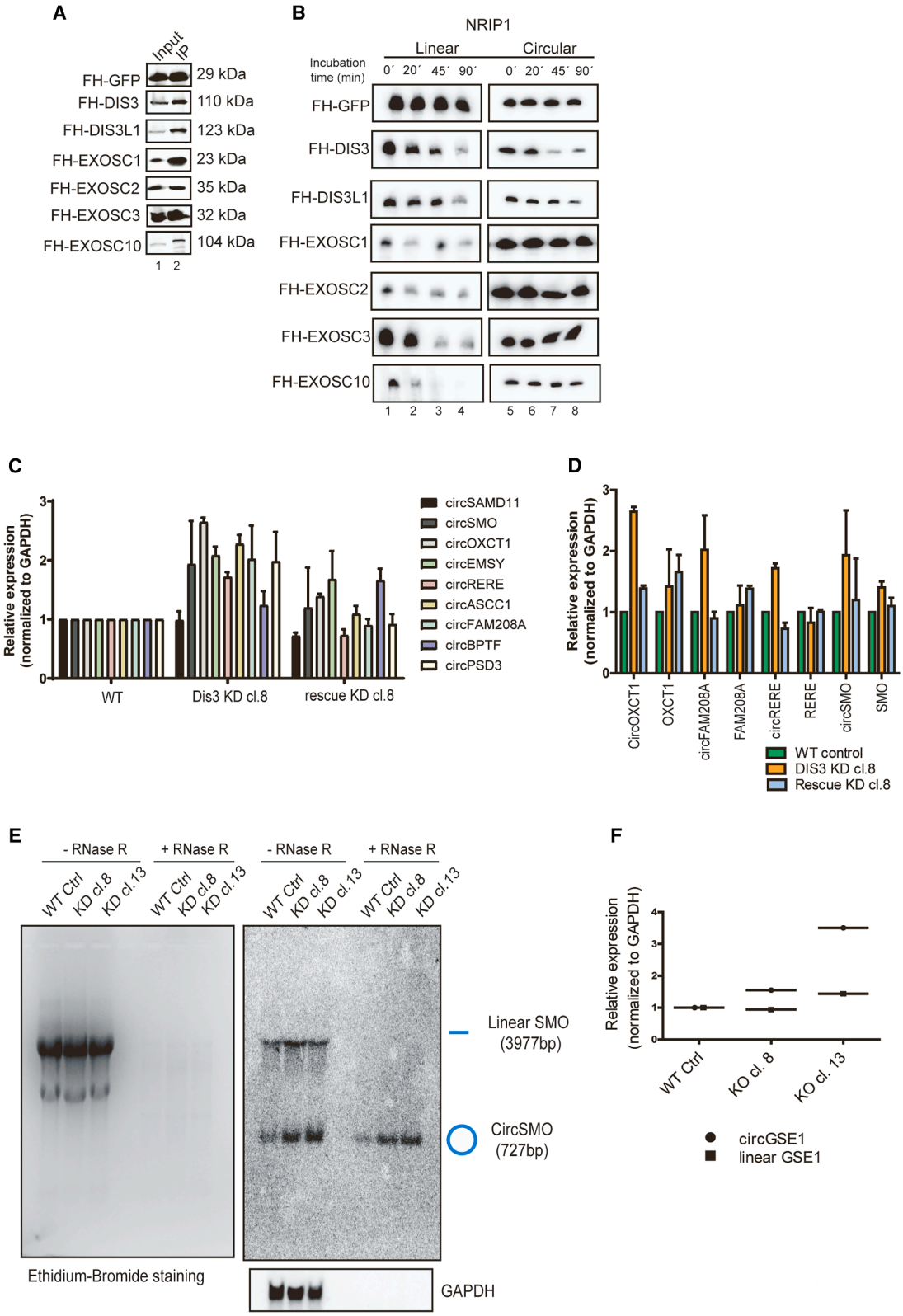

(legend on next page)

immunofluorescence and stained fixed HEK293 cells with antibodies against DIS3 (Figure 4A). Similarly to what has been reported earlier,[20] we found most DIS3 in the nucleus but also a weaker signal in the cytoplasm. Next, we fractionated nuclear and cytoplasmic extracts and used western blotting against DIS3 (Figure 4B). Consistently, DIS3 is found in both nuclear and cytoplasmic fractions. Furthermore, when we assessed the localization of endogenous circRNAs in these lysates using qPCR (Figure 4C), we found the analyzed circRNAs predominantly in the cytoplasmic fractions, which would be in line with cytoplasmic degradation by DIS3.

When cell lysates were fractionated by glycerol density centrifugation (Figure 4D), the majority of DIS3 migrated in low-molecular-weight fractions confirming the presence of cleavage activity in these fractions as we initially observed (Figure 1). Core exosome components (EXOSC3, 9, and 10) co-migrate at a higher density with only a minor overlap with DIS3 (Figure 4D). It is known that DIS3 transiently binds to the exosome, and interactions are lost in lysates under high salt conditions.[20] Interestingly, DIS3L1, which interacts with the exosome through its catalytically inactive PIN domain, migrates in higher molecular weight fractions under these conditions, where core exosome components are found as well (Figure 4D), suggesting that salt concentrations might not lead to DIS3/DIS3L1 dissociation from the exosome. DIS3L2, which lacks a PIN domain and does not bind to the exosome, served as negative control and migrates similarly to DIS3. To further strengthen the hypothesis that DIS3 functions partially independent of the exosome, we performed co-immunoprecipitations assays using the core exosome component EXOSC9 under high and low salt conditions (Figure 4E). Consistent with the fractionation experiments (Figure 4D), a minor fraction of DIS3 co-immunoprecipitates with EXOSC9 under both low and high salt conditions. DIS3L1, however, efficiently interacts with EXOSC9 under both conditions (Figure 4E).

Taken together, our results suggest the catalytic activity of the cytoplasmic pool of DIS3 toward circRNA, which is, unlike nuclear DIS3 or DIS3L1, independent of associating with the core exosome.

DISCUSSION

CircRNAs are generated from a large variety of exons, and thousands of such back-splicing events have been observed. We therefore hypothesized that circRNAs might be cleaved by housekeeping endoribonucleases independent of their nucleotide sequence. Indeed, we find that the exo-/endoribonuclease DIS3, which is mainly nuclear and associated with the exosome, can use its PIN domain to cleave circRNAs. It has been shown before that the PIN domain of DIS3 is catalytically active,[21–23] but the cellular targets remained poorly understood. We find that human DIS3 functions as a stand-alone endoribonuclease that can target naturally occurring circRNAs *in vitro* independently of associating with the exosome. Since circRNAs (or structured RNA substrates) could not get through the exosome channel, an exosome-independent function of the DIS3 PIN domain appears likely. Using biochemical fractionations, we observe that circRNA-degrading activity is found in the cytoplasmic fractions. Although human DIS3 is enriched in the nucleus, a smaller pool is also found in the cytoplasm in immunofluorescence studies (Figure 3A).[20] It is clearly present in cytoplasmic fractionations supporting the model of DIS3-mediated cytoplasmic circRNA cleavage. Thus, our work assigns a role to the so far enigmatic cytoplasmic DIS3 pool. Interestingly, nuclear fractions also contain DIS3 but appear much less active in our circRNA degradation assays. It is conceivable that nuclear DIS3 could be specifically modified, for example, and indeed, using mass spectrometry, we find that DIS3 is generally highly phosphorylated (Figure S4). Extensive phosphorylation has also been observed for fission yeast DIS3.[24] Whether these phosphorylation sites affect RNA targeting or exosome association will be an exciting direction for future studies. Another speculation could be that either circRNAs interact with nuclear proteins that protect them from DIS3 degradation or DIS3 itself interacts with nuclear proteins (potentially even the exosome itself) that would prevent circRNA recognition and degradation in our biochemical lysates. Another puzzling question is how DIS3 discriminates between circRNAs and linear RNAs in the cytoplasm. RNP compositions and RNA structures might prevent DIS3 cleavage, and certain circRNAs might be more accessible. However, this speculation needs to be proven in future studies.

We observed a clear circRNA cleavage activity *in vitro* and also in northern blot analyses using DIS3 partial knockout cells, where we observed a mild but detectable effect of DIS3 on circSMO. Strikingly, a study by Tao et al.[25] used a very comprehensive RNA sequencing approach and clearly found a large circRNA population that is affected by DIS3 knockdown. It is nevertheless tempting to speculate that certain low-abundant circRNAs might simply be splicing by-products. Low molecule numbers might result in limited contact with the decay machinery and might even be tolerated under steady-state conditions in

Figure 3. DIS3 reduction affects circRNA levels in cells

(A) FLAG-HA (FH)-tagged exosome components were immunoprecipitated from HEK293 cell lysates and detected by western blot using anti-HA antibodies.

(B) Cleavage assays using radiolabeled linear and circular NRIP1 and the indicated resin-immobilized FH-tagged proteins at different time points. FH-GFP served as negative control.

(C) RNA was isolated from Flp-T-Rex 293 cell lines (WT, DIS3 KD cl.8, rescue DIS3 KD cl.8 with WT DIS3), and circRNA levels were analyzed by quantitative reverse-transcription PCR (RT-qPCR). GAPDH expression levels served for data normalization. All bar plots show mean ± SD from two biological replicates.

(D) Selected circRNA and linear RNA expression levels were compared by RT-qPCR in DIS3 KD cl.8 and in the corresponding rescue DIS3 WT cells by adding doxycycline. GAPDH expression levels served for data normalization. All bar plots show mean ± SD from two biological replicates.

(E) RNA was isolated from Flp-T- Rex 293 cell lines (WT, DIS3 KD cl.8 and cl.13) and treated with RNase R. Northern blot analyses showing linear and circular SMO expression in DIS3-depleted cells. GAPDH mRNA was used as control. Dash, linear SMO; circle, circSMO. The probe used spans the splice junction of circSMO.

(F) The circular and linear SMO signal intensities were calculated following GAPDH normalization and phosphorimager analysis and are indicated in the graph.

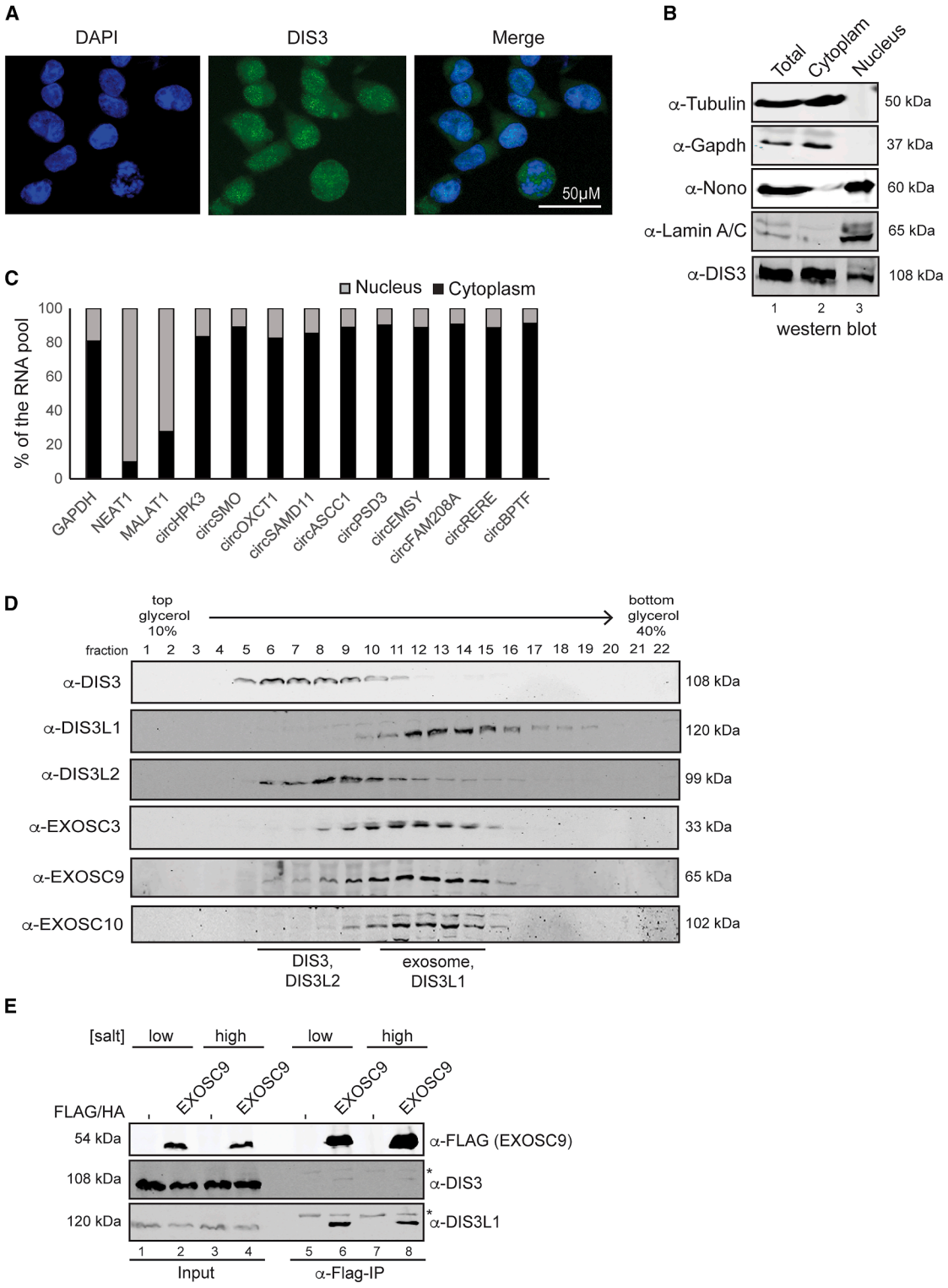

Figure 4. Cytoplasmic DIS3 degrades circRNA independently of the exosome

(A) Immunofluorescence of endogenous DIS3 in HEK293 cells using anti-DIS3 antibodies (green). Nuclei were stained with DAPI (blue) (scale bars: 50 μm).

(B) Nuclear and cytoplasmic fractionation of HEK293 cell lysates. Western blot analysis of the distribution of DIS3 in the subcellular fractions. Gapdh was used as cytoplasmic marker, while Lamin A/C and Nono served as nuclear markers. Endogenous DIS3 was detected using a specific antibody.

(legend continued on next page)

tissue culture cells. Terminally differentiated cells such as neurons that accumulate such RNAs over a long lifetime[26] might be a system where such degradation mechanisms become more physiologically important and should be envisioned in future experiments.

Finally, other endoribonucleases likewise also contribute to specific circRNA degradation processes. Beyond the reported enzymes, we identified a number of potential endoribonucleases in the active fractions. Among them, ARD1 was tested further and shows also effects in *in vitro* assays (Figure S2B). Thus, it is likely that not only DIS3 but potentially also other endoribonucleases could cleave circularized RNAs when they become abundant and accessible. Vice versa, some circRNA could have acquired specific functions during evolution, and levels of such circRNAs might be specifically regulated through distinct endoribonucleases. These speculations, however, require further investigation.

Limitations of the study

Our study provides mechanistic insights into so far unrecognized cytoplasmic roles of DIS3. Nevertheless, biochemical *in vitro* studies have limitations. *In vitro* cleavage of labeled circRNAs in cellular lysates with many other nucleases present is technically challenging, and therefore, contaminating background degradation is frequently observed. *In vitro* cleavage assays provide mechanistic insights but may not fully reflect conditions in cells, where compartmentalization, for example, could affect activity. Furthermore, we generated DIS3 knockout cells with significant leaky expression of an inducible rescue construct. Whether this leaky expression already leads to circRNA degradation and negatively affects our studies in cells is unclear and is thus a limitation.

RESOURCE AVAILABILITY

Lead contact

Requests for further information, resources, and reagents should be directed to and will be fulfilled by the lead contact, Gunter Meister (gunter.meister@ur.de).

Materials availability

All unique/stable reagents generated in this study are available from the lead contact with a completed materials transfer agreement.

Data and code availability

- All mass spectrometry data reported in this paper are publicly available at the protein exchange platform under the accession number: PXD050442, project webpage: https://www.ebi.ac.uk/pride/archive/projects/PXD050442.
- This paper does not report original code.
- Data reported in this paper will be shared by the lead contact upon request.
- Any additional information required to reanalyze the data reported in this paper is available from the lead contact upon request.

ACKNOWLEDGMENTS

We thank S. Ammon, C. Friederich, and the mass spectrometry group for excellent support. This work was in part supported by the Deutsche Forschungsgemeinschaft (DFG) grant TRR305 and the European Research Council (ERC grant 682291 "moreRNA"). G.M. was supported by the BMBF in the framework of the Cluster4Future program (Cluster for Nucleic Acid Therapeutics Munich, CNATM) (Project ID: 03ZU1201BD).

AUTHOR CONTRIBUTIONS

C.L. and J.E. performed most experiments, A.-L.F. produced recombinant proteins, S.-N.Z. analyzed the data, H.H.-X. contributed to the experiments, G.L. analyzed the data, P.G. analyzed the data, N.R. discussed the experiments and analyzed the data, A.B. performed mass spectrometry, L.Y. discussed the experiments and analyzed the data, R.S. discussed the data and experiments, G.M. designed and discussed the experiments, and C.L. and G.M. wrote the manuscript.

DECLARATION OF INTERESTS

The authors declare no competing interests.

STAR★METHODS

Detailed methods are provided in the online version of this paper and include the following:

- KEY RESOURCES TABLE
- EXPERIMENTAL MODELS
  - Mammalian cells
  - Generation of stable inducible Flp-In T-REx -293 cell lines
  - Generation of DIS3 knockout cell lines
- METHOD DETAILS
  - Immunofluorescence
  - RNA isolation and qRT-PCR
  - *In vitro* RNA transcription, circularization and purification
  - RNase R treatment
  - RNase H treatment
  - RNA degradation assays
  - ^{32}P-labeling of oligonucleotides or cDNA probes
  - Northern blot on polyacrylamide gels and agarose gels
  - Whole cell lysis and nuclear and cytoplasmic cell fractions
  - Ammonium sulfate cuts of cytoplasmic extracts
  - Glycerol gradient
  - Transfections
  - Immunoprecipitation and western blotting
  - Protein preparation
  - Mass spectrometric analysis
  - Plasmids
  - Analysis of clones from CRISPR/CAS9 editing
- QUANTIFICATION AND STATISTICAL ANALYSIS

(C) Quantification of the nuclear/cytoplasmic localization of selected circRNAs by RT-qPCR. Gapdh was used as cytoplasmic marker and the long non-coding RNAs MALAT1 and NEAT1 as nuclear markers. Bar plots represent percentages of examined circRNAs and linear RNAs in each subcellular fraction from two biological replicates.
(D) Total lysates from HEK293 cells were separated by glycerol density gradient centrifugation. Endogenous DIS3, DIS3L1, and DIS3L2 and several core exosome components were detected using specific antibodies.
(E) FLAG-HA (FH)-tagged EXOSC9 was immunoprecipitated from HEK293 cell lysates at low (75 mM KCl) and high (150 mM KCl) salt conditions and detected by western blot using an anti-FLAG antibody. Endogenous co-immunoprecipitated DIS3 and DIS3L1 proteins were detected using specific antibodies.

SUPPLEMENTAL INFORMATION

Supplemental information can be found online at https://doi.org/10.1016/j.celrep.2025.115769.

Received: March 10, 2024
Revised: March 28, 2025
Accepted: May 9, 2025

REFERENCES

1. Yang, L., Wilusz, J.E., and Chen, L.L. (2022). Biogenesis and Regulatory Roles of Circular RNAs. Annu. Rev. Cell Dev. Biol. *38*, 263–289. https://doi.org/10.1146/annurev-cellbio-120420-125117.
2. Fica, S.M., and Nagai, K. (2017). Cryo-electron microscopy snapshots of the spliceosome: structural insights into a dynamic ribonucleoprotein machine. Nat. Struct. Mol. Biol. *24*, 791–799. https://doi.org/10.1038/nsmb.3463.
3. Liang, D., Tatomer, D.C., Luo, Z., Wu, H., Yang, L., Chen, L.L., Cherry, S., and Wilusz, J.E. (2017). The Output of Protein-Coding Genes Shifts to Circular RNAs When the Pre-mRNA Processing Machinery Is Limiting. Mol. Cell *68*, 940–954.e3. https://doi.org/10.1016/j.molcel.2017.10.034.
4. Ashwal-Fluss, R., Meyer, M., Pamudurti, N.R., Ivanov, A., Bartok, O., Hanan, M., Evantal, N., Memczak, S., Rajewsky, N., and Kadener, S. (2014). circRNA biogenesis competes with pre-mRNA splicing. Mol. Cell *56*, 55–66. https://doi.org/10.1016/j.molcel.2014.08.019.
5. Hansen, T.B., Jensen, T.I., Clausen, B.H., Bramsen, J.B., Finsen, B., Damgaard, C.K., and Kjems, J. (2013). Natural RNA circles function as efficient microRNA sponges. Nature *495*, 384–388. https://doi.org/10.1038/nature11993.
6. Memczak, S., Jens, M., Elefsinioti, A., Torti, F., Krueger, J., Rybak, A., Maier, L., Mackowiak, S.D., Gregersen, L.H., Munschauer, M., et al. (2013). Circular RNAs are a large class of animal RNAs with regulatory potency. Nature *495*, 333–338. https://doi.org/10.1038/nature11928.
7. Kristensen, L.S., Andersen, M.S., Stagsted, L.V.W., Ebbesen, K.K., Hansen, T.B., and Kjems, J. (2019). The biogenesis, biology and characterization of circular RNAs. Nat. Rev. Genet. *20*, 675–691. https://doi.org/10.1038/s41576-019-0158-7.
8. Legnini, I., Di Timoteo, G., Rossi, F., Morlando, M., Briganti, F., Sthandier, O., Fatica, A., Santini, T., Andronache, A., Wade, M., et al. (2017). Circ-ZNF609 Is a Circular RNA that Can Be Translated and Functions in Myogenesis. Mol. Cell *66*, 22–37.e9. https://doi.org/10.1016/j.molcel.2017.02.017.
9. Pamudurti, N.R., Bartok, O., Jens, M., Ashwal-Fluss, R., Stottmeister, C., Ruhe, L., Hanan, M., Wyler, E., Perez-Hernandez, D., Ramberger, E., et al. (2017). Translation of CircRNAs. Mol. Cell *66*, 9–21.e7. https://doi.org/10.1016/j.molcel.2017.02.021.
10. Kristensen, L.S., Hansen, T.B., Venø, M.T., and Kjems, J. (2018). Circular RNAs in cancer: opportunities and challenges in the field. Oncogene *37*, 555–565. https://doi.org/10.1038/onc.2017.361.
11. Liu, C.X., Li, X., Nan, F., Jiang, S., Gao, X., Guo, S.K., Xue, W., Cui, Y., Dong, K., Ding, H., et al. (2019). Structure and Degradation of Circular RNAs Regulate PKR Activation in Innate Immunity. Cell *177*, 865–880.e21. https://doi.org/10.1016/j.cell.2019.03.046.
12. Park, O.H., Ha, H., Lee, Y., Boo, S.H., Kwon, D.H., Song, H.K., and Kim, Y.K. (2019). Endoribonucleolytic Cleavage of m(6)A-Containing RNAs by RNase P/MRP Complex. Mol. Cell *74*, 494–507.e8. https://doi.org/10.1016/j.molcel.2019.02.034.
13. Fischer, J.W., Busa, V.F., Shao, Y., and Leung, A.K.L. (2020). Structure-Mediated RNA Decay by UPF1 and G3BP1. Mol. Cell *78*, 70–84.e6. https://doi.org/10.1016/j.molcel.2020.01.021.
14. Lasda, E., and Parker, R. (2016). Circular RNAs Co-Precipitate with Extracellular Vesicles: A Possible Mechanism for circRNA Clearance. PLoS One *11*, e0148407. https://doi.org/10.1371/journal.pone.0148407.
15. Li, W.M., Barnes, T., and Lee, C.H. (2010). Endoribonucleases–enzymes gaining spotlight in mRNA metabolism. FEBS J. *277*, 627–641.
16. Kilchert, C., Wittmann, S., and Vasiljeva, L. (2016). The regulation and functions of the nuclear RNA exosome complex. Nat. Rev. Mol. Cell Biol. *17*, 227–239. https://doi.org/10.1038/nrm.2015.15.
17. Sloan, K.E., Schneider, C., and Watkins, N.J. (2012). Comparison of the yeast and human nuclear exosome complexes. Biochem. Soc. Trans. *40*, 850–855. https://doi.org/10.1042/BST20120061.
18. Pirouz, M., Munafò, M., Ebrahimi, A.G., Choe, J., and Gregory, R.I. (2019). Exonuclease requirements for mammalian ribosomal RNA biogenesis and surveillance. Nat. Struct. Mol. Biol. *26*, 490–500. https://doi.org/10.1038/s41594-019-0234-x.
19. Kobylecki, K., Drazkowska, K., Kulinski, T.M., Dziembowski, A., and Tomecki, R. (2018). Elimination of 01/A'-A0 pre-rRNA processing by-product in human cells involves cooperative action of two nuclear exosome-associated nucleases: RRP6 and DIS3. RNA *24*, 1677–1692. https://doi.org/10.1261/rna.066589.118.
20. Tomecki, R., Kristiansen, M.S., Lykke-Andersen, S., Chlebowski, A., Larsen, K.M., Szczesny, R.J., Drazkowska, K., Pastula, A., Andersen, J.S., Stepien, P.P., et al. (2010). The human core exosome interacts with differentially localized processive RNases: hDIS3 and hDIS3L. EMBO J. *29*, 2342–2357. https://doi.org/10.1038/emboj.2010.121.
21. Lebreton, A., Tomecki, R., Dziembowski, A., and Séraphin, B. (2008). Endonucleolytic RNA cleavage by a eukaryotic exosome. Nature *456*, 993–996. https://doi.org/10.1038/nature07480.
22. Schaeffer, D., Tsanova, B., Barbas, A., Reis, F.P., Dastidar, E.G., Sanchez-Rotunno, M., Arraiano, C.M., and van Hoof, A. (2009). The exosome contains domains with specific endoribonuclease, exoribonuclease and cytoplasmic mRNA decay activities. Nat. Struct. Mol. Biol. *16*, 56–62. https://doi.org/10.1038/nsmb.1528.
23. Schneider, C., Leung, E., Brown, J., and Tollervey, D. (2009). The N-terminal PIN domain of the exosome subunit Rrp44 harbors endonuclease activity and tethers Rrp44 to the yeast core exosome. Nucleic Acids Res. *37*, 1127–1140. https://doi.org/10.1093/nar/gkn1020.
24. Telekawa, C., Boisvert, F.M., and Bachand, F. (2018). Proteomic profiling and functional characterization of post-translational modifications of the fission yeast RNA exosome. Nucleic Acids Res. *46*, 11169–11183. https://doi.org/10.1093/nar/gky915.
25. Tao, X., Zhai, S.N., Liu, C.X., Huang, Y., Wei, J., Guo, Y.L., Liu, X.Q., Li, X., Yang, L., and Chen, L.L. (2025). Degradation of circular RNA by the ribonuclease DIS3. Mol. Cell *85*, 1674–1685.e8. https://doi.org/10.1016/j.molcel.2025.01.012.
26. Rybak-Wolf, A., Stottmeister, C., Glažar, P., Jens, M., Pino, N., Giusti, S., Hanan, M., Behm, M., Bartok, O., Ashwal-Fluss, R., et al. (2015). Circular RNAs in the Mammalian Brain Are Highly Abundant, Conserved, and Dynamically Expressed. Mol. Cell *58*, 870–885. https://doi.org/10.1016/j.molcel.2015.03.027.
27. Meister, G., Landthaler, M., Patkaniowska, A., Dorsett, Y., Teng, G., and Tuschl, T. (2004). Human Argonaute2 Mediates RNA Cleavage Targeted by miRNAs and siRNAs. Mol. Cell *15*, 185–197.
28. Fuchs, A.L., Wurm, J.P., Neu, A., and Sprangers, R. (2020). Molecular basis of the selective processing of short mRNA substrates by the DcpS mRNA decapping enzyme. Proc. Natl. Acad. Sci. USA *117*, 19237–19244. https://doi.org/10.1073/pnas.2009362117.
29. Ran, F.A., Hsu, P.D., Wright, J., Agarwala, V., Scott, D.A., and Zhang, F. (2013). Genome engineering using the CRISPR-Cas9 system. Nat. Protoc. *8*, 2281–2308. https://doi.org/10.1038/nprot.2013.143.

STAR★METHODS

KEY RESOURCES TABLE

REAGENT or RESOURCE	SOURCE	IDENTIFIER
Antibodies		
Mouse monoclonal anti-HA.11 antibody (clone 16B2)	Covance	Cat# MMS-101P, RRID:AB_2314672
Mouse monoclonal anti-beta actin antibody (ab6276)	Abcam	Cat# ab6276, RRID:AB_2223210
Rabbit polyclonal anti-beta Tubulin antibody (ab87651)	Abcam	Cat# ab87651, RRID:AB_1952658
Rabbit monoclonal anti-GAPDH (FL-335)	Santa Cruz Biotechnologies	Cat# sc-25778, RRID:AB_10167668
Mouse monoclonal anti-p54[nrb]	BD Transduction Laboratories	Cat# 611278, RRID:AB_398806
Mouse monoclonal anti-FLAG®M2 (F3165)	Sigma	Cat# F3165, RRID:AB_259529
Rabbit polyclonal Lamin A/C (H-110)	Santa Cruz Biotechnologies	Cat# sc-20681, RRID:AB_648154
Rabbit polyclonal DIS3 (A303-765A)	Bethyl laboratories	Cat# A303-765A RRID:AB_11205807
Mouse monoclonal EXOSC9 (67636-1-Ig)	Proteintech	Cat# 67636-1-Ig, RRID:AB_2882837
Rabbit polyclonal EXOSC3 (A303-909A)	Bethyl laboratories	Cat# A303-909A RRID:AB_2620259
Rabbit polyclonal EXOSC10 (11178-1-AP)	Proteintech	Cat# 11178-1-AP RRID:AB_2293792
Rabbit polyclonal DIS3L	Proteintech	Cat# 25746-1-AP RRID: AB_2880222
Rabbit polyclonal DIS3L2	Proteintech	Cat# 67623-1-Ig RRID: AB_2882825
Goat polyclonal anti-mouse IgG, IRDye 800CW conjugated antibody	LI-COR Bioscience	Cat#925–32210; RRID: AB_2687825
Goat polyclonal anti-rabbit IgG, IRDye 800CW conjugated antibody	LI-COR Bioscience	Cat#926–32211; RRID: AB_621843
Goat polyclonal anti-mouse IgG, IRDye 680CW conjugated antibody	LI-COR Bioscience	Cat#926–68070; RRID: AB_10956588
Goat polyclonal anti-rabbit IgG, IRDye 680CW conjugated antibody	LI-COR Bioscience	Cat# 926–32221, RRID:AB_621841
Bacterial and virus strains		
XL1 blue competent cells	this paper	N/A
Chemicals, peptides, and recombinant proteins		
RNA T7 Polymerase	this paper	N/A
T4 Polynucleotide Kinase (T4 PNK)	Thermo Fisher Scientific	Cat#EK0031
RiboLock RNase Inhibitor	Thermo Fisher Scientific	Cat#EO0384
Proteinase K	Thermo Fisher Scientific	Cat#AM2546
Blasticidin	Gibco	Cat#A1113903
Zeocin	Invitrogen	Cat#R25001
Hygromycin B	Invitrogen	Cat#10687010
Tetracycline	AppliChem	Cat#A2228.0025
Penicillin/Streptomycin	Sigma	Cat#P0781
AEBSF	Sigma Aldrich	Cat#A8456
Calf intestinal alkaline phosphatase	New England Biolabs Sigma Aldrich	Cat#M0290
T4 RNA ligase 1	New England Biolabs	Cat#11705
RNase H	Thermo Scientific	Cat# EN0201
RNAse R	Epicenter	Cat# MRNA092
Lipofectamin™ 2000	Invitrogen	Cat#11668500

(*Continued on next page*)

Continued

REAGENT or RESOURCE	SOURCE	IDENTIFIER
Coomassie Brilliant Blue R250	BioRad	Cat#1610436
SimpleBlue™SafeStain	Thermo Scientific	Cat#LC6060
EDC (1-ethyl-3-(3-dimethylaminopropyl) - carbodiimide hydrochloride)	Sigma Aldrich	Cat#E7750; CAS: 25952-53-8
1-Methylimidazole	Sigma-Aldrich	Cat#M50834; CAS: 616-47-7
γ-^{32}P-ATP	Hartmann Analytic	Cat#FP-501
illustra™ MicroSpin G-25 column	GE Healthcare	Cat#27532501
ANTI-FLAG M2 Affinity Gel	Sigma Aldrich	Cat#A2220
Phenol/Chloroform/Isoamylalcohol	Roth	Cat#A156.1
TRIzol	Invitrogen	Cat#15596018
TRIzol LS	Invitrogen	Cat#10296010
Critical commercial assays		
Phusion® High-Fidelity DNA Polymerase	New England BioLabs®	Cat#M0530L
NucleoSpin Gel and PCR Clean-up kit	Macherey-Nagel	Cat#740609.50
NucleoSpin Mini Plasmid, Mini kit	Macherey-Nagel	Cat#740588.50
NucleoBond Xtra Midi EF, Midi kit	Macherey-Nagel	Cat#740422.50
NucleoSpin RNA, Mini kit for RNA purification	Macherey-Nagel	Cat# 740955.50
NuPAGE 4–12% Bis-Tris protein gels	Invitrogen	Cat#NP0321PK2
First-strand cDNA synthesis kit	Thermo Fisher Scientific	Cat#K1612
Takyon™ No ROX SYBR 2x MasterMix blue dTTP	Eurogentec	Cat#NA.55
T4 Polynucleotide Kinase (T4 PNK) kit – Buffer A	Thermo Fisher Scientific	Cat#EK0031
Deposited data		
Mass spectrometric analysis of nucleases candidates	this paper	PXD050442, Project https://doi.org/10.6019/PXD050442
Experimental models: Cell lines		
Human: Flp-In™TREx™ -293	ATCC	Cat# CRL-1573, RRID:CVCL_0045
Human: HEK293T	Our laboratory	RRID: CVCL_0063
Oligonucleotides		
DNA oligonucleotide for qRT-PCR, see Table 1. Table of used oligonucleotides, related to STAR Methods	Metabion	N/A
Northern blot probe sequences, see Table 1. Table of used oligonucleotides, related to STAR Methods	Metabion	N/A
DNA oligonucleotide sequences for cloning see Table 1. Table of used oligonucleotides, related to STAR Methods	Metabion	N/A
DNA oligonucleotide sequences for *in vitro* transcription, see Table 1. Table of used oligonucleotides, related to STAR Methods	Metabion	N/A
DNA oligonucleotide for RNase H assay see Table 1. Table of used oligonucleotides, related to STAR Methods	Metabion	N/A
Recombinant DNA		
pcDNA™5/FRT/TO modified with N-terminal F/H-tag	Invitrogen	Cat#V652020
pOG44	Invitrogen	Cat#V600520
pcDNA™5/FRT/TO FH-DIS3	this paper	N/A
pX459 sgRNA DIS3 intron-guide RNA1	this paper	N/A
pX459 sgRNA DIS3 intron-guide RNA2	this paper	N/A
pIRES-VP5 modified	Meister et al.[27]	N/A
pIRES-VP5-FH-DIS3	this paper	N/A
pIRES-VP5-FH-ARD1	this paper	N/A
pIRES-VP5-FH-EXOSC1	this paper	N/A
pIRES-VP5-FH-EXOSC2	this paper	N/A

(*Continued on next page*)

Continued

REAGENT or RESOURCE	SOURCE	IDENTIFIER
pIRES-VP5-FH-EXOSC3	this paper	N/A
pIRES-VP5-FH-EXOSC10	this paper	N/A
pIRES-VP5-FH-DIS3L1	this paper	N/A
Software and algorithms		
Quantity One Software	BioRad	Quantity One 1-D Analysis Software, RRID:SCR_014280
Uniprot		UniProtKB, RRID:SCR_004426
FastQC (version 0.11.9)		FastQC, RRID:SCR_014583
Odyssey	LI-CORE	Odyssey CLx, RRID:SCR_014579
NCBI database		NCBI, RRID:SCR_006472
CFX96real-Time System BioRad	BioRad	N/A
Personal Molecular Imager™ System	BioRad	N/A
Protein Scape 3.1.3	Bruker Daltonics	N/A
Data Analysis 4.2	Bruker Daltonics	N/A
Mascot 2.5.1	Matrix Science	RRID: SCR_014322

EXPERIMENTAL MODELS

Mammalian cells

The HEK 293T cells (female, embryonic kidney) were grown in Dulbecco's modified Eagle's medium (DMEM; Sigma Aldrich) supplemented with 10% fetal bovine serum (FBS; Gibco), 100 U/mL penicillin, and 100 mg/mL streptomycin (Sigma) under standard condition at 37°C and 5% CO2. The Flp-In T-Rex 293 cells were obtained from the American Type Culture Collection (ATCC). The medium was further supplemented with 15 μg/mL blasticidin (Gibco) and 100 μg/mL zeocin (Invitrogen). Flp-In T-REx 293 cell lines stably expressing Flag/HA-DIS3 and their derived knockout cells were supplemented with 15 μg/mL blasticidin (Gibco) and 150 μg/mL hygromycin B (Invitrogen).

Generation of stable inducible Flp-In T-REx -293 cell lines

Stable inducible cell lines were generated using the Flp-In T-REx 293 system. Briefly, Flp-In T-REx 293 cell lines were seeded into 6-well plate and co-transfected with pOG44 plasmid and pcDNA™5/FRT/TO in a 9:1 ratio. Transfection was carried out by Lipofectamin™ 2000 (Invitrogen) reagent according to the manufacture's protocol. After 48 h, cells were transferred into a 10 cm plate and selected using 15 μg/mL blasticidin and 150 μg/mL hygromycin B. Single clones were picked approximately two weeks later and tested by western blot for the expression of Flag/HA-DIS3 upon induction with Doxycycline (1 μg/mL). Stable clones were maintained in the same medium as used for selection.

Generation of DIS3 knockout cell lines

DIS3 knockout cell lines were generated from Flp-In T-Rex 293 stable cell lines using the Dual-guide CRISPR/Cas9-directed genome editing. Briefly, two guide RNAs were used simultaneously to generate two double-strand breaks to delete the DIS3 exon containing the PIN domain. Cells were transfected with PX459 plasmid expressing the two guide RNAs using Lipofectamin™ 2000 (Invitrogen) reagent according to the manufacture's protocol. 24 h post-transfection, the cells were selected with complete medium containing 6 μg/mL puromycin. After one day of selection, the medium was replaced with DMEM in order to make recovery the resistant cells. When the cells were confluent, a second forward transfection was performed followed by another puromycin selection. After the recovering step, the cells were sorted into 96-well plates. Single clones were expanded into 6-well plate and tested for knockout by genomic PCR and western blot.

METHOD DETAILS

Immunofluorescence

HEK 293 cells for immunofluorescence analysis were grown on coverslips. After 24 h HEK 293 cells were fixed with 4% formaldehyde solution in PBS for 10 min at 37°C. Fixation was stopped by PBS +100 mM glycine for 5 min. Cells were then washed by PBS +0.2% Triton X-100 for 15 min at room temperature. After another washing step, glass slides were incubated in blocking solution (PBS +0.05% Triton X-100 + 1% BSA) at RT for 1 h, followed by overnight incubation at 4°C with primary antibody (PBS +0.05% Triton X-100 + 1% BSA). After three washing steps with PBS +0.05% Triton X-100 + 1% BSA the secondary antibody was added

and incubated for 1 h at room temperature. Cells were then washed once with PBS +0.05% Triton X-100 + 1% BSA and twice with PBS and mounted using Prolong Gold + DAPI (Life Technologies). Images were recorded on Keyence Fluorescence BZ-X800 Series Microscope.

RNA isolation and qRT-PCR

RNA extraction from mammalian cells was performed with TRIzol reagent (Life Technologies) or NucleoSpin RNA Kit (Macherey-Nagel) following the manufacturer's protocol. RNAs were reversed transcribed by First-strand cDNA synthesis kit (Thermo Fisher Scientific) using random primer. Fluorometric amplification was performed by Takyon™ No ROX SYBR 2x MasterMix blue dTTP (Eurogentec) and CFX96real-Time System (BioRad). Data were evaluated using the $2^{-\Delta\Delta CT}$ method and normalized to control sample. Primer sequences are listed in Table S2.

In vitro RNA transcription, circularization and purification

Linear RNAs were *in vitro* transcribed from PCR amplified DNA containing the T7 promoter sequence. Primer sequences are listed in Table S2. Briefly, 1 μg of PCR-amplified DNA template was incubated with 0.1 mg/mL T7 RNA polymerase in 1x T7 reaction buffer (30 mM Tris pH 8.0, 10 mM DTT, 0.01% [v/v] Triton X-100, 25 mM $MgCl_2$, 2 mM spermidine, 30% [v/v] DMSO, 5 mM ADP, 5 mM CTP, 5 mM UTP, 5 mM GTP, 0.4 U/ml thermostable inorganic pyrophosphatase (NEB)) overnight at 37°C. Afterwards, the reaction was digested with 1 μL of 1 U/unit DNase I (Thermo Scientific) for 15 min at 37°C to remove DNA templates. *In vitro* transcribed RNAs were purified by 6% urea-PAGE gel and visualized by UV-shadowing. Corresponding bands were excised and eluted in RNA elution buffer (300 mM NaCl, 2 mM EDTA) overnight at 4°C in agitation. RNAs were precipitated with 100% ethanol and washed twice with 80% [v/v] ethanol and resuspended in RNase-free water.

To produce 5′-monophosphate RNA necessary for *in vitro* circularization, 10 μg of linear transcribed RNAs were incubated with 2.5 μL of 10 U/μl Alkaline Phosphatase, Calf Intestinal (CIP) (NEB) and 1 μL RiboLock RNase Inhibitor (Thermo Scientific) for 1 h at 37°C. Dephosphorylated RNAs were precipitated by phenol-chloroform and resuspended in RNase-free water. Prior circularization, dephosphorylated linear RNAs were phosphorylated with 20 μCi of γ-^{32}P-ATP (Hartmann Analytic) or 10 mM ATP, 0.5 U/ml T4 Polynucleotide Kinase (PNK), 1 μL RiboLock in 1x PNK buffer A (Thermo Scientific) at 37°C for 30 min. Phosphorylated RNAs were purified by phenol-chloroform extraction as previously described. Before phenol-chloroform extraction, ^{32}P labeled RNAs were previously purified with G-25 columns (GE Healthcare).

For *in vitro* circularization, phosphorylated linear RNAs or ^{32}P labelled linear RNAs were incubated in 1x T4 RNA ligase buffer with 50 U T4 RNA ligase (NEB), 10 mM ATP and 1 μL RiboLock overnight at 16°C. Reaction products were resolved in 6% denaturing urea polyacrylamide gel and visualized by ethidium bromide staining for phosphorylated RNAs or by storage phosphor screens and Personal Molecular Imager™ System (BioRad) with Quantity One Software (version 4.6.9, Bio-Rad) for ^{32}P labeled linear RNAs. Circular RNA gel bands were excised and eluted in RNA elution buffer overnight at 4°C with shaking. Circular RNAs were precipitated with 100% ethanol and resuspended in RNase-free water. Purified circular or linear RNAs were validated by RNase R or RNase L treatments.

RNase R treatment

50 ng purified linear or circular RNA were treated with 0.1 U RNase R (Epicentre) in 10 μL 1x RNase R reaction volume for 20 min at 37°C. After the addition of 2x RNA sample buffer (99,9% Formamide, 0.025% Xylene cyanol, 0.025% Bromphenol blue in TBE), RNA was resolved on 6% denaturing urea polyacrylamide gel and detected by northern blot.

RNase H treatment

RNase H assays were performed in 15 μL total reaction volume. 100 ng of purified linear or circular RNA and 1 μL of 10 μM antisense oligonucleotide were denatured 2 min at 95°C, 2 min at 75°C and slowly cooled down at 37° C. Oligonucleotide sequences are listed in Table S2. 1x RNase H (Thermo Scientific) buffer was added followed by incubation at 37°C for 20 min 2.5 U RNase H (Thermo Scientific) was added followed by incubation at 37°C for an additional 40 min. After the addition of 2x RNA sample buffer (99,9% Formamide, 0.025% Xylene cyanol, 0.025% Bromphenol blue in TBE), RNA was separated by 6% denaturing urea polyacrylamide gel and detected by northern blot.

RNA degradation assays

In vitro enzymatic degradation assays were performed in 20 μL reaction volumes containing 10 mM Tris-HCl pH 8.0, 75 mM NaCl, and 1 mM 2-mercaptoethanol with $MnCl_2$ at final concentration of 3 mM or with $MgCl_2$ at final concentration of 0.5 mM. 1 Bq/cm^2 of ^{32}P labelled linear or circular RNAs and 0.1 mM of purified proteins or 20 μL resin-immobilized immunoprecipitated proteins were used. Reaction mixtures were incubated at 37°C for the indicated time points and stopped with the addiction of 1 volume of 2x RNA sample buffer (99,9% Formamide, 0.025% Xylene cyanol, 0.025% Bromphenol blue in TBE) supplemented with 20 mM EDTA. Reactions products were purified or directly resolved in 6% polyacrylamide urea gels. Radioactive signals were detected by storage phosphor screens and Personal Molecular Imager System (BioRad) with Quantity One Software (version 4.6.9, Bio-Rad).

^{32}P-labeling of oligonucleotides or cDNA probes

DNA oligonucleotides used for Northern blot probes (Table S2), were labeled by incubating 20 pmol of oligonucleotides with 20 μCi of γ-^{32}P-ATP (Hartmann Analytic) and 0.5 U/μl T4 PNK in 1x PNK buffer A (Thermo Scientific) for 30–60 min incubation at 37°C. The reaction was then stopped by adding 30 μL of a 30 mM EDTA solution (pH 8.0). Unincorporated nucleotides were separated on a G-25 column (GE Healthcare) according to the manufacturer's instructions.

The cDNA probes were prepared using Megaprime DNA-Labelling Systems kit (Amersham). Afterward, the reaction was stopped with 5 μL of 200 mM EDTA. The cDNA probes were purified using the Illustra MicroSpin G-25. cDNA probes were denatured by heating at 95°C for 5 min and then immediately placed on ice for 5 min.

Northern blot on polyacrylamide gels and agarose gels

25 ng of synthetized linear and circular RNA were resolved in 1x TBE on 6% polyacrylamide (acrylamide/bisacrylamide 19:1) urea gels (Carl Roth). After electrophoresis, RNA was stained with ethidium bromide, blotted for 30 min at 20 V onto an Amersham Hybond-N membrane (GE Healthcare) and crosslinked to the membrane for 1 h at 50°C using an EDC solution. An additional UV-crosslinking (254 nm, 120 mJoule/cm^2) was performed in a UV Stratalinker (Stratagene). Membrane was incubated overnight in Hybridization solution (20 mM sodium phosphate buffer pH 7.2, 5x SSC, 1% SDS, 2% Denhardt's solution) with a ^{32}P-labeled DNA oligonucleotide antisense at 50°C overnight. After 12–15 h the membrane was washed twice with washing solution I (5x SSC, 1% SDS) and once with washing solution II (1x SSC, 1% SDS) at 50°C for 10 min. Radioactive signals were detected by exposure to phosphor screens and using the Personal Molecular Imager™ System (BioRad) with the Quantity One Software (version 4.6.9, Bio-Rad).

20 μg of total RNA was mixed with 2x RNA loading buffer (45% Formamide, 1x MOPS, 2% Formaldehyde, 5% Glycerol, 0.01% Bromophenol Blue) and 1μL of EtBr (400 μg/μL) and resolved in 1x MOPS on 1% agarose gel containing 1x MOPS buffer and 2% Formaldehyde (37%). After electrophoresis, RNA was visualized by UV-shadowing. The agarose gels were washed in 50 mM NaOH for 30 min, in 50 mM Tris pH 7.5 for 30 min and in 20x SSC for 30 min. RNA was transferred onto a Hybond-N membrane by capillary transfer using 20x SSC. The transfer was set at room temperature overnight, preferably for 18 h. The RNA was crosslinked to the membrane using the UV Stratalinker at 254 nm. After crosslinking, the membrane was incubated overnight in Hybridization solution with ^{32}P-labeled cDNA probes at 60°C. After 12–15 h, the membrane was washed 30 min with washing solution III (2x SSC, 0.1% SDS), 30 min with washing solution IV (0.5x SSC, 0.1% SDS) and another 30 min with washing solution V (0.1x SSC, 0.1% SDS) at 60°C. Radioactive signals were detected by storage phosphor screens and Personal Molecular Imager™ System (BioRad) with Quantity One Software (version 4.6.9, Bio-Rad).

Whole cell lysis and nuclear and cytoplasmic cell fractions

Whole cells were generally lysed in IP lysis buffer (25 mM Tris-HCl pH 7.4, 150 mM KCl, 0.5% NP-40, 2 mM EDTA, 1 mM NaF,1 mM AEBSF and 1 mM DTT and incubated on ice for 20 min. Cells were centrifuged at 17,000 xg for 20 min at 4°C. The supernatant was collected and subjected to immunoprecipitation experiments or directly loaded onto a SDS gel.

For Nuclear and Cytoplasmic extracts, cells were lysed in hypotonic lysis buffer (HBL) (10 mM Tris-HCl pH 7.5, 10 mM NaCl, 3 mM $MgCl_2$, 0.3% NP-40, 1 mM AEBSF and 1 mM DTT) and incubated on ice for 8 min 1 mL of HBL was use for every 75 mg of cells. After incubation, cells were centrifuged at 800 xg at 4° for 8 min. The supernatant was kept as cytoplasmic fraction. The nuclei pellet was washed four time with HBL by centrifuging at 200 xg for 2 min. The nuclei pellet was resuspended in nuclear lysis buffer (NLB) (10 mM Tris-HCl pH 7.5, 150 mM KCl, 3 mM $MgCl_2$, 0.3% NP-40, 1 mM AEBSF and 1 mM DTT). 0.5 mL of NLB was used for every 75 mg of initial cells. Nuclei were sonicated on ice 1-3 times at 20% power for 15 s and kept as nuclear fraction. Cytoplasmic and nuclear fractions were additionally centrifuged at 15000 xg for 15 min at 4°C and the supernatants were transferred in new tubes.

Ammonium sulfate cuts of cytoplasmic extracts

For ammonium sulfate precipitation, saturated ammonium sulfate solution was added to the cytoplasmic extracts at the indicated final percentages (20%, 30% and 50%) and stirred at 4°C for 30 min. The samples were then centrifuged at 10000 xg for 10 min. The pellets were dissolved in PBS and the supernatants was kept for the next AS cuts. Additional saturated AS solution was added to the supernatants to raise 10% or 20% higher percentages of saturation. The samples were stirred for 30 min at 4°C and centrifuged at 10000 g for 10 min. The pellets were the 20-30%, 30-50% and 50-70% saturated AS cuts. The pellets were dissolved in PBS and dialysed overnight. The different AS cuts were tested for *in vitro* RNA degradation assays with the addition of 5 mM ATP and 7.5 mM $MgCl_2$.

Glycerol gradient

A 10% to 40% glycerol gradient solution was prepared in 150 mM KCl, 50 mM Tris/HCl pH 7.5 and 5 mM $MgCl_2$ using a 14 × 89mm ultracentrifuge tube and the Bio Comp Gradient Master instrument (long cap, 10-40% glycerol v/v). Ammonium sulfate cuts or cell extracts were separated by high-velocity sedimentation through the 10% to 40% glycerol gradient at 40,000 rpm, 4°C for 18 h using the SW40 Ti rotor. Fractions of approximately 500-700 μL were collected manually and tested for enzymatic degradation assays or loaded onto an SDS gel.

Transfections

For immunoprecipitations of overexpressed proteins, HEK 293 cells were plated and transfected 3-4 h later using the calcium phosphate method. Therefore, 10 μg of plasmid DNA for each cell culture dish with a diameter of 15 cm was used. Cells were harvested after 48 h.

Transfections for the generation of knockout cell lines or stable HEK293 T-REx cell lines were performed with Lipofectamine 2000 (Invitrogen) according to the manufacturer's instructions.

Immunoprecipitation and western blotting

FH-tagged proteins were precipitated with 30 μL of Anti-FLAG M2 affinity gel (Sigma-Aldrich). For each immunoprecipitation reaction, 80-90% confluent cells were harvested from one to two cell culture dishes (150 mm diameter). Cell lysis was performed in 1 mL IP lysis buffer (20 mM Tris/HCl pH 7.5, 150 mM KCl, 2 mM EDTA, 1 mM NaF, 0.5% NP-40) supplemented with 1 mM DTT and 1 mM AEBSF. 10% of protein lysate was used as input control. The remaining lysate was incubated with the beads under constant rotation for 2-3 h at 4°C. The beads were washed four times with ice-cold IP wash buffer (20 mM Tris/HCl pH 7.5, 300 mM KCl, 1 mM $MgCl_2$, 0.5% NP-40) and once with ice-cold PBS. The beads were resuspended in 100 μL of PBS or of degradation buffer. A 20 μL aliquot was taken for western blot analysis. In case of IP experiments performed at low salt conditions, KCl concentrations in the IP lysis and wash buffers were reduced to 75 mM.

Proteins were mixed with 4x Laemmli buffer. Samples were boiled at 95°C for 5 min and separated by a 10% SDS-PAGE gel. Proteins were transferred onto a nitrocellulose membrane (0.45 μm, GE Healthcare) by semi dry blotting (SD Semi-Dry Transfer Cell, Bio-RAD). Nitrocellulose membrane was blocked in TBS containing 5% milk for 1 h at RT and subsequently incubated with the primary antibody overnight at 4°C with agitation. After 3 washing steps with TBS-Tween, the secondary antibody was applied for 1 h at RT. Signals were detected by Odyssey Infrared Imaging System (LI-COR Biosciences). Gels were stained by Coomassie Blue (0.25% Coomassie Brilliant Blue R250 (Bio-Rad), 10% acetic acid, 30% ethanol) and cleansed afterward with destainer solution (10% acetic acid, 30% ethanol). For mass spectrometry analysis, proteins were separated on 4%–12% NUPAGE Bis-Tris gels (Invitrogen) using MOPS buffer. Gels were stained with Simply Blue colloidal Coomassie blue G250 (Invitrogen).

Protein preparation

For the production of Rrp44 or Rrp44 PIN domains or variants thereof BL21 (DE3) *Escherichia coli* cells were transformed with a plasmid (obtained from Genscript and codon optimized for bacterial overexpression; point mutants were introduced using the quick-change approach) that codes for the respective protein plus a Tobacco etch virus (TEV) cleavable N-terminal His6-tag. Cells were grown in lysogeny broth medium at 37°C to OD_{600} = 0.6. Subsequently, protein expression was induced with 0.5 mM isopropyl β-*d*-1-thiogalactopyranoside and cells were shifted to 20°C for 16 h. Cells were harvested by centrifugation and resuspended in buffer A (50 mM NaPO4, pH 8.0, 150 mM NaCl, 5 mM Imidazole) supplemented with 0.1% Triton X-100, 1 mM ethylenediaminetetraacetic acid, and lysozyme. After lysis by sonication, 2 mM $MgSO_4$ was added, insoluble cell debris removed by centrifugation, and the supernatant was applied to Ni-NTA resin that was equilibrated in buffer A. The resin was washed with buffer A, and the protein was eluted with buffer B (buffer A supplemented with 200 mM Imidazole). The eluted protein was supplemented with 0.5 mg of TEV protease and simultaneously dialyzed against 25 mM Tris pH 8.0, 75 mM NaCl, 1 mM dithiothreitol (DTT) at 4°C. The cleaved affinity tag and TEV protease were removed by reverse Ni-affinity chromatography, after which the proteins were subjected to size exclusion chromatography on a Superdex S200 column (GE Healthcare) in 20 mM HEPES pH 7.5, 200 mM NaCl, 1 mM DTT.

The *S. cerevisiae* exo-9 complex was overexpressed from a single plasmid that carried the coding regions for all nine exosome core proteins,[28] where the Rrp4 protein contains an N-terminal His6-TEV tag. The complete exo-9 complex was purified using Ni-NTA resin and size exclusion chromatography as described above for Rrp44. The final exo-9 sample contained all nine proteins in equimolar amounts. The catalytically active exo-10 complex was prepared by mixing equimolar amounts of the exo-9 complex and Rrp44. The final exo-10 complex was obtained after an additional size-exclusion chromatography step in 20 mM HEPES pH 7.5, 200 mM NaCl, 1 mM DTT.

Mass spectrometric analysis

For mass spectrometric analysis of proteins gel lanes were cut into consecutive slices. The gel slices were then transferred into 2 mL microtubes (Eppendorf) and washed with 50 mM NH_4HCO_3, 50mM NH_4HCO_3/acetonitrile (3:1) and 50mM NH_4HCO_3/acetonitrile (1:1) while shaking gently in an orbital shaker (VXR basic Vibrax, IKA). Gel pieces were lyophilized after shrinking by 100% acetonitrile. To block cysteines, reduction with DTT was carried out for 30 min at 57°C followed by an alkylation step with iodoacetamide for 30 min at room temperature in the dark. Subsequently, gel slices were washed and lyophilized again as described above. Proteins were subjected to *in gel* tryptic digest overnight at 37°C with approximately 2 μg trypsin per 100 μL gel volume (Trypsin Gold, mass spectrometry grade, Promega). Peptides were eluted twice with 100 mM NH_4HCO_3 followed by an additional extraction with 50 mM NH_4HCO_3 in 50% acetonitrile. Prior to LC-MS/MS analysis, combined eluates were lyophilized and reconstituted in 20 μL of 1% formic acid. Separation of peptides by reversed-phase chromatography was carried out on an UltiMate 3000 RSLCnano System (Thermo Scientific, Dreieich) which was equipped with a C18 Acclaim Pepmap100 preconcentration column (100μm i.D.x20mm, Thermo Fisher) in front of an Acclaim Pepmap100 C18 nano column (75 μm i.d. × 150 mm, Thermo Fisher). A linear gradient of 4%–40% acetonitrile in 0.1% formic acid over 90 min was used to separate peptides at a flow rate of 300 nL/min. The LC-system

was coupled on-line to a maXis plus UHR-QTOF System (Bruker Daltonics, Bremen) via a CaptiveSpray nanoflow electrospray source (Bruker Daltonics). Data-dependent acquisition of MS/MS spectra by CID fragmentation was performed at a resolution of minimum 60000 for MS and MS/MS scans, respectively. The MS spectra rate of the precursor scan was 2 Hz processing a mass range between m/z 175 and m/z 2000. Via the Compass 1.7 acquisition and processing software (Bruker Daltonics) a dynamic method with a fixed cycle time of 3 s and an m/z dependent collision energy adjustment between 34 and 55 eV was applied. Raw data processing was performed in Data Analysis 4.2 (Bruker Daltonics), and Protein Scape 3.1.3 (Bruker Daltonics) in connection with Mascot 2.5.1 (Matrix Science) facilitated database searching of the Swiss-Prot *Homo sapiens* database (release-2020_01, 220420 entries). Search parameters were as follows: enzyme specificity trypsin with 1 missed cleavage allowed, precursor tolerance 0.02 Da, MS/MS tolerance 0.04 Da, carbamidomethylation or propionamide modification of cysteine, oxidation of methionine, deamidation of asparagine and glutamine were set as variable modifications. Mascot peptide ion-score cut-off was set 15. If necessary, fragment spectra were validated manually. Protein list compilation was done using the Protein Extractor function of Protein Scape.

Plasmids

Expression of FLAG-HA-tagged protein was achieved from modified pIRES-VP5 (VP5) plasmids[27] encoding N-terminal FLAG/HA tag. The open reading frame (ORF) of human DIS3 was PCR-amplified from cDNA using oligonucleotides NotI-DIS3-Fw and AscI-DIS3-Rev.The PCR product was digested with NotI and AscI and was inserted into VP5 generating VP5-FH-DIS3. The VP5 constructs encoding FH-ARD1, FH-EXOSC1, FH-EXOSC2, FH-EXOSC3, FH-EXOSC10 and FH-DIS3L1 were created by PCR-amplification of the ORF from human cDNA using the relative primer pairs FseI- PPP1R8/ARD1-Fw and AscI- PPP1R8/ARD1-Rev; FseI-EXOSC1-Fw and AscI-EXOSC1-Rev; FseI-EXOSC2-Fw and AscI-EXOSC2-Rev; FseI-EXOSC3-Fw and AscI-EXOSC3-Rev; FseI-EXOSC10-Fw and AscI-EXOSC10-Rev FseI-DIS3L1-Fw and AscI-DISL1-Rev. The PCR products were digested with FseI and AscI and inserted into VP5 generating VP5-FH-ARD1, VP5-FH-EXOSC1, VP5-FH-EXOSC2, VP5-FH-EXOSC3, VP5-FH-EXOSC10 and VP5-FH-DIS3L1. Primer sequences are listed in Table S2.

The pcDNA5/FRT/TO + FH-DIS3 WT plasmid was generated by PCR-amplification of the DIS3 construct from VP5 plasmids using the primer pairs BamHI-DIS3-fw and XhoI-DIS3-fw and by ligation into a modified pcDNA5/FRT/TO vector already containing the N-terminal FH-tag and a modified multiple cloning site.

Genome editing was achieved with gene excision by Dual-Guide CRISPR-Cas9 system. To this end, guide sequences against the DIS3 gene were designed and ligated into the pSpCas9(BB)-2A-Puro (PX459) V2.0 vector[29] created by the Zhang group. Briefly, the PIN domain of DIS3 was deleted from the genome by directing the Cas9 endonuclease upstream and downstream of the PIN exon sequence. To avoid co-transfection of distinct plasmids, the two independent single-guide RNAs targeting the intronic regions of the PIN domain of DIS3 were cloned in a single PX459 V2.0 plasmid using the following guides: DIS3-intron-guideRNA1-sense, DIS3-intron-guideRNA1-antisense and the DIS3-intron-guideRNA2-sense, DIS3-intron-guideRNA2-antisense. Guide sequences are listed in Table S2.

Analysis of clones from CRISPR/CAS9 editing

To analyze if gene editing by CRISPR/CAS9 had been successful, specific primers were designed to generate a PCR-amplicon of about 677 bp flanking the deletion region (Table S2).

For preparation of genomic DNA from clonal cell lines, cells were resuspended in 500 μL proteinase K buffer (300 mM NaCl, 200 mM Tris-HCl, pH 7.5, 25 mM EDTA, 2% (w/v) SDS) containing 0.2 mg/mL proteinase K and incubated at 50°C overnight. DNA was precipitated by adding 400 μL 2-propanol and centrifugation for 30 min at 21,000 xg and 4°C. The cell pellet was resuspended in 500 μL Proteinase K buffer and incubated o/n at 50°C. 400 μL isopropanol was added and the mixture was incubated for 1 h at −20°C. The sample was centrifuged for 15 min at full speed and the supernatant was discarded. The pellet was washed once with 1 mL 70% ethanol. The gDNA pellet was air-dried and dissolved in 100 μL H_2O by shaking at 500 rpm o/n at 37°C and used for PCR reaction. The reaction protocol consisted of an initial denaturation step at 98°C for 30″, followed by 30 cycles with a 10″ denaturation step at 98°C, a 30″ annealing step at the 62°C and an elongation step at 72°C for 10''. The reaction was ended with a final elongation step at 7°C for 3 min.

QUANTIFICATION AND STATISTICAL ANALYSIS

Mean values and SD values were calculated using Prism software (GraphPad). Please refer to the figure legends or the method details for description of sample size and statistical analyses.